Influence of the crystallization process on the luminescence of multilayers of SiGe nanocrystals embedded in SiO_2

M. Avella , Á.C. Prieto , J. Jiménez , A. Rodríguez , J. Sangrador , T. Rodríguez , M.I. Ortiz , C. Ballesteros

Dpto. Física de la Materia Condensada, E.T.S.I. Industriales, Universidad de Valladolid, 47011 Valladolid, Spain
Dpto. Tecnología Electrónica, E.T.S.I. de Telecomunicación, Universidad Politécnica de Madrid, 28040 Madrid, Spain
Dpto. Física, E.P.S., Universidad Carlos III, 28911 Leganés, Madrid, Spain

Abstract

Multilayers of SiGe nanocrystals embedded in an oxide matrix have been fabricated by low-pressure chemical vapor deposition of SiGe and SiO_2 onto Si wafers (in a single run at 390 °C and 50 mTorr, using GeH_4, Si_2H_6 and O_2) followed by a rapid thermal annealing treatment to crystallize the SiGe nanoparticles. The main emission band is located at 400 nm in both cathodoluminescence and photoluminescence experiments at 80 K and also at room temperature. The annealing conditions (temperatures ranging from 700 to 1000 °C and for times of 30 and 60 s) have been investigated in samples with different diameter of the nanoparticles (from ≈3 to ≥5 nm) and oxide interlayer thickness (15 and 35 nm) in order to establish a correlation between the crystallization of the nanoparticles, the degradation of their composition by Ge diffusion and the intensity of the luminescence emission band. Structures with small nanoparticles (3–4.5 nm) separated by thick oxide barriers (≈35 nm) annealed at 900 °C for 60 s yield the maximum intensity of the luminescence. An additional treatment at 450 °C in forming gas for dangling-bond passivation increases the intensity of the luminescence band by 25–30%.

Keywords: SiGe nanocrystals; LPCVD; Crystallization; Transmission electron microscopy; Raman spectroscopy; Cathodoluminescence

1. Introduction

Group IV (Si or Ge) nanocrystals embedded in SiO_2 have applications in non-volatile memories and optoelectronic devices fully compatible with the CMOS technology
For these applications, the diameter of the nanoparticles should be uniform and of a few nanometers, and their spatial distribution must be regular and with a nanoparticle areal density above 5×10^{11} cm^{-2}. SiGe nanocrystals, with controlled composition and size and the appropriate areal density, embedded in an oxide matrix have been obtained by low-pressure chemical vapor deposition (LPCVD) of amorphous discontinuous SiGe films followed by an annealing process to crystallize the nanoparticles These structures show luminescence emission with a main band peaking at a wavelength of 400 nm unambiguously associated to the presence of the crystallized nanoparticles

In this work, the effect of the post-growth annealing processes for nanoparticle crystallization has been investigated in samples with different diameter of the SiGe nanoparticles and thickness of the SiO_2 interdielectric layers (IDL) with the aim of establishing a correlation between the crystallization of the SiGe nanoparticles and the optimal conditions for the luminescence emission.

2. Experimental

2.1. Samples preparation

Multilayer structures with five periods of amorphous SiGe nanoparticles/SiO_2 and a top SiO_2 capping layer were deposited to increase the areal density of nanoparticles. The deposition processes were carried out in a commercial hot tube LPCVD reactor operating at a low constant temperature of 390 °C and a total pressure of 50 mTorr according to the procedures described elsewhere The SiGe nanoparticles, with a Ge fraction of $x \approx 0.4$, were deposited using Si_2H_6 and GeH_4 with a gas flow

Table 1
Structural features of the three samples, diameter (d) of the SiGe nanoparticles and thickness (t) of the SiO_2 IDL

Sample	d (nm)	t (nm)
S-1	≥ 5	35
S-2	3–4.5	15
S-3	3–4.5	35

ratio of $GeH_4/Si_2H_6 = 0.82$. The SiO_2 layers were deposited using Si_2H_6 and O_2 with a flow ratio of $Si_2H_6/O_2 = 0.2$. Three types of samples were fabricated (see Table 1), with amorphous SiGe nanoparticles of different diameters (d) and IDL of different thicknesses (t) obtained by varying the deposition times of both materials. The crystallization of the nanoparticles was achieved by subsequent rapid thermal annealing of the samples in N_2 atmosphere at temperatures between 700 and 1000 °C and for times of 30 and 60 s. Selected samples were further annealed in an open tube furnace at 450 °C for 30 min exposed to a high flow of forming gas (10% H_2 + 90% N_2). Pure SiO_2 films were also deposited and annealed in the same conditions than the $SiGe/SiO_2$ multilayers to be used as control samples.

2.2. Characterization techniques

Analytical Transmission electron microscopy (TEM) with high resolution (HRTEM) was used in cross sections of the samples to study the distribution of the nanoparticles, to determine their size and areal density and to analyze their crystallization. The studies were carried out using a Philips Tecnai 20F FEG microscope operating at 200 kV, equipped with an energy dispersive X-ray (EDX) analysis system. Electron diffraction pattern simulation using fast Fourier transform (FFT) of the HREM images and subsequent filtering were used to improve the contrast. Raman spectroscopy was used to analyze the crystallization of the nanoparticles. The spectra were acquired using a Jobin Yvon HR Labram spectrometer operating in backscattering geometry. The excitation was done with the 325 nm line of a He–Cd laser and the detection was performed with a liquid nitrogen cooled CCD multichannel detector. The cathodoluminescence (CL) emission of the samples was measured in a XiCLOne system (Gatan) attached to a SEM (JEOL 820). The spectra were measured at LN_2 temperature using an e-beam acceleration voltage of 5 kV and a beam current of 10 nA. Photoluminescence (PL) measurements were also carried out at room temperature in selected samples using the 325 nm line of a He–Cd laser and a liquid nitrogen cooled CCD camera detector.

3. Results

3.1. Transmission electron microscopy

Fig. 1 shows cross-section TEM and HREM images of samples S-1, S-2 and S-3 after annealing at 900 °C for 60 s. The morphology of the samples after annealing remains unaltered compared to the as-deposited ones (not shown), preserving the average nanoparticle density. In sample S-1, due to the two-dimensional projection of the three-dimensional sample, the layers appear to be continuous. Higher magnification studies carried out in very thin areas indicate that the layers are discontinuous, although the areal density of nanoparticles could not be estimated because the nanoparticles appear superimposed to each other in the images. EDX spectra obtained in very thin areas of the as-deposited samples indicate that the atomic Ge fraction of the nanoparticles is consistent with the expected value $x \approx 0.4$. The minimum areal density of nanoparticles in samples S-2 and S-3 are always above 5×10^{11} cm^{-2} in each layer. The nanoparticles of the sample S-2 appear to be crystallized after the thermal treatment, whereas an incomplete crystallization was observed in some of the nanoparticles of sample S-3. EDX spectra acquired in the as-deposited S-2 and S-3 samples show that the nanoparticles, deposited with the same flow ratio used in sample S-1, contain Ge. FFT images show that the lattice parameter of the nanocrystals is intermediate between those of Si and Ge. However, a quantitative analysis of the composition was not possible in these cases.

3.2. Raman spectroscopy

Fig. 2 displays Raman spectra of the three samples after different annealing processes, showing the first order bands related to Ge–Ge (275–300 cm^{-1}), Si–Ge (375–400 cm^{-1}) and Si–Si ($\approx$475 cm^{-1}) bond vibrations and, in S-2 and S-3, the band due to crystalline Si (520.2 cm^{-1}) arising from the Si substrate (in S-1 the excitation beam does not reaches the substrate).

In sample S-1, with large nanoparticles, one observes the Raman signature of crystallized SiGe after annealing at a temperature as low as 700 °C. For increasing annealing temperature and time, the three Raman bands of SiGe are sharpened, their intensities increase and their peak wavenumbers are shifted, which obeys the progressive crystallization of the nanoparticles. Stresses and compositional changes could also contribute to shift the Raman bands, but it is difficult to separate the different contributions. No further improvement of the crystallization is detected after annealing at 900 °C for times above 60 s. The Raman signature of SiGe disappears for an annealing temperature of 1000 °C.

In sample S-2, with smaller nanoparticle size, one observes the crystallization at temperatures of 800 °C or higher, in agreement with the crystallization data reported for pure Ge nanocrystals of a size equivalent that of our nanoparticles [8,9]. No further crystallization is detected if the annealing is prolonged at a fixed temperature. To detect any progress in the crystallization of the nanoparticles, the annealing temperature needs to be increased. At 1000 °C the Raman bands of SiGe are not present in the spectra. The intensity of the Ge–Ge band, relative to that of the other two bands, decreases for high temperature and long-time annealing processes, which reveals a slight reduction of the Ge fraction of the nanocrystals. The Raman bands of these samples are broader than those observed for sample S-1, a result that can be associated with phonon con-

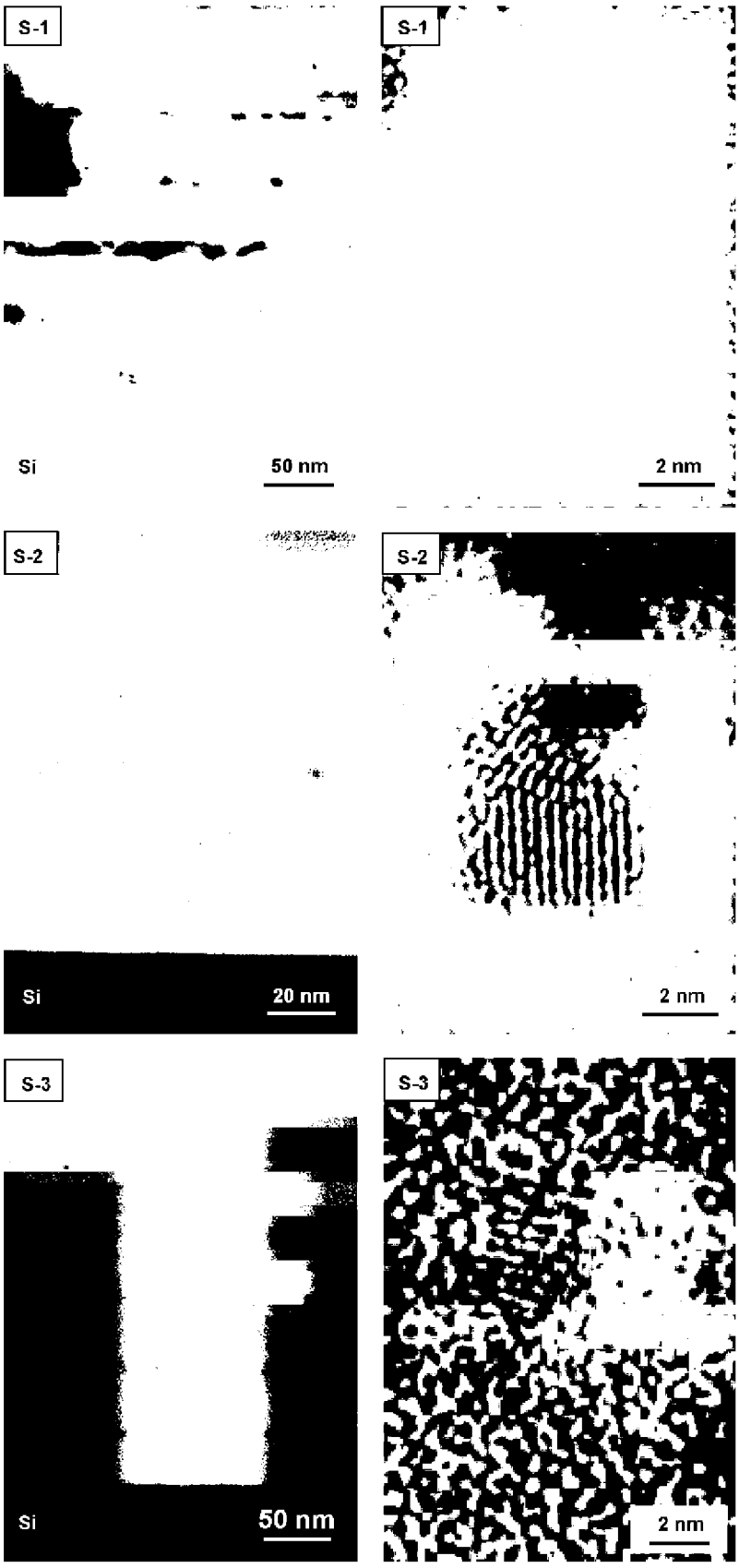

Fig. 1. Cross-sectional TEM (left) and HRTEM (right) images of samples S-1, S-2 and S-3 annealed at 900 °C for 60 s showing the SiGe (dark)/SiO_2 (bright) multilayers and a detail of a SiGe nanocrystal, respectively.

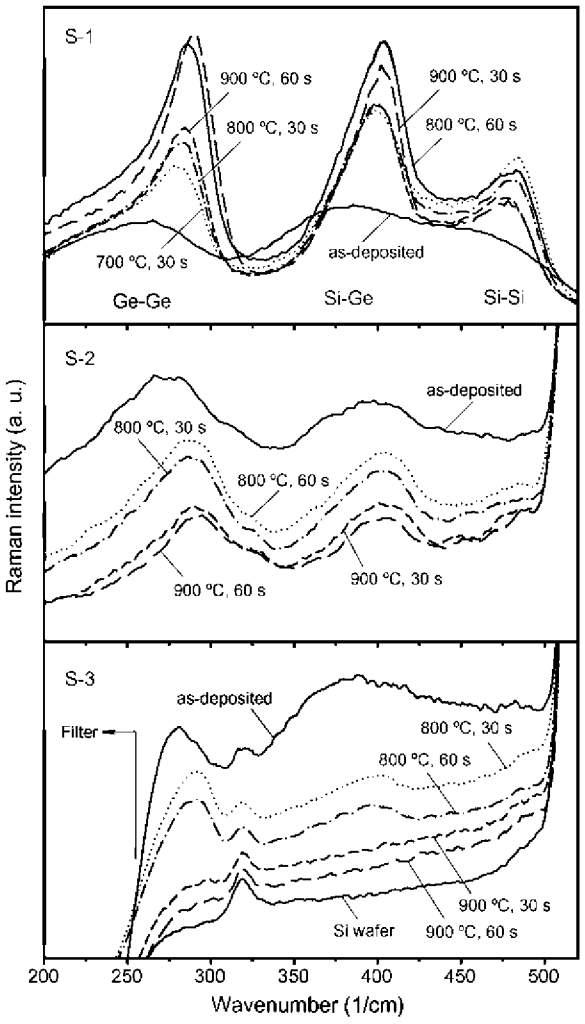

Fig. 2. Raman spectra of samples S-1, S-2 and S-3 as-deposited and annealed in different conditions. The spectra of S-3 have been shifted for clarity. A filter inserted during the acquisition of the spectra of S-3 is the cause of their shape below 250 cm^{-1}. The peak at 320 cm^{-1} is due to the instrument.

finement, which is significant for particle sizes smaller than 5 nm

For S-3, the Raman signature of SiGe appears in the spectra of the samples as-deposited and annealed at 800 °C, but it is not observed at all in the spectra of the samples annealed at 900 °C. Since the TEM images reveal the presence of the SiGe nanocrystals, the non-observation of the Raman spectrum of SiGe in these samples can be interpreted as a consequence of the widening of the band gap due to quantum confinement, which drastically reduces the efficiency of the Raman scattering. The same effect is found if the spectrum of samples containing nanocrystals of any size and with a given band gap is acquired using an excitation of lower energy (i.e. the 514.5 nm line of an Ar^+ laser) Possible contributions to the band gap widening in the nanocrystals of sample S-3 are on one side the smaller crystallite size, which is probably due to partial crystallization (see Fig. 1), and the improvement of the crystalline quality by increasing the annealing temperature. These results suggest that the band gap of the nanocrystals of sample S-3 annealed at 900 °C is wider than 4 eV.

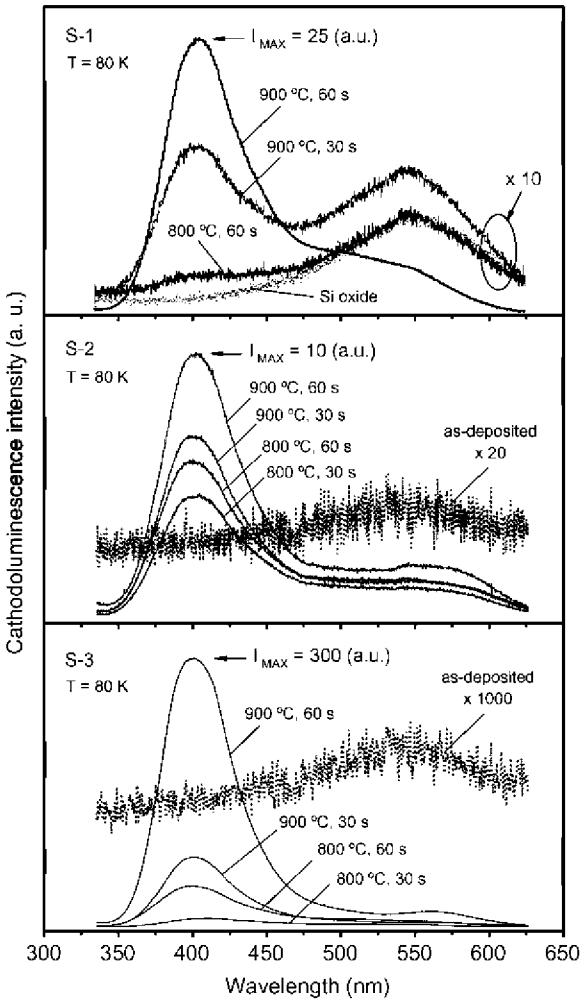

Fig. 3. Cathodoluminescence spectra measured at 80 K of samples S-1, S-2 and S-3 as-deposited and annealed in different conditions. The spectrum of the annealed oxide (control sample) is included.

3.3. Cathodoluminescence spectroscopy

Fig. 3 shows the CL spectra of samples S-1, S-2 and S-3 as-deposited and after different annealing treatments as well as the spectra of a pure oxide layer annealed at 900 °C during 60 s (control sample). The main spectral feature of the annealed samples is the violet band peaking at around 400 nm, which is fully absent in the spectra of the as-deposited samples and of the control sample (annealed oxide). Therefore, this band appears correlated to the presence of the SiGe nanocrystals inside the oxide matrix. The intensity of the band depends on the characteristics of the samples, which are related to their structure (nanocrystal size and IDL thickness) and the thermal treatments. The peak wavelength, 400 nm, does not shift for the different samples, which have nanocrystals of different diameters, ruling out any quantum confinement effect in the mechanism responsible for the luminescence emission. This luminescence band is probably related to Ge oxygen deficient centers (GeODC) formed at the interface of the SiGe nanocrystals with the oxide matrix, since the same band has also been observed in samples with pure Ge nanocrystals embedded in an oxide matrix

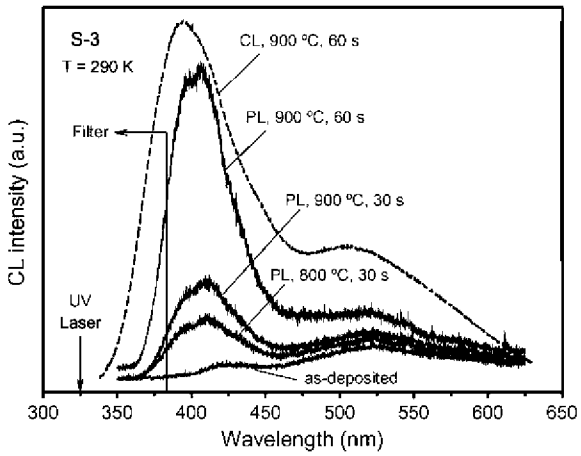

Fig. 4. Photoluminescence spectra measured at 290 K of sample S-3 annealed in different conditions and a CL spectrum, also measured at 290 K, of the sample S-3 annealed at 900 °C for 60 s. A filter inserted during the measurements is responsible for the shape of the spectra below 385 cm^{-1}.

In sample S-1 the CL band starts to be observed after annealing at 800 °C for 60 s, while crystallization is detected at 700 °C after 30 s. According to this, the enhancement of the luminescence emission appears to be correlated with an improvement of the crystallinity. In sample S-2 the CL band appears after annealing at 800 °C for 30 s, the same conditions that induce detectable crystallization. The intensity of the CL band increases with the annealing temperature and time, but the maximum value reached after annealing at 900 °C for 60 s is smaller than in the other two samples. One can argue that the reduction of the Ge fraction of the nanocrystals observed by Raman spectroscopy, which is probably due to Ge diffusion favored by the thin IDL of this sample, should lead to a concomitant reduction of the GeODC centers at the interfaces. In sample S-3, intense CL is measured after annealing at 900 °C for 60 s. The high intensity of the luminescence emission can be due to the small size of the nanocrystals, with the corresponding reduction of the crystal defects, which reduces the contribution of the competitive non-radiative recombination paths associated with those crystal defects.

An additional thermal treatment in forming gas at 450 °C causes an increase in the intensity of the luminescence band by around 25–30% (not shown). The effect of this treatment in an atmosphere containing H_2 is the passivation of the dangling bonds in the nanocrystals, thus reducing the amount of non-radiative recombination centers.

3.4. Photoluminescence spectroscopy

Fig. 4 shows photoluminescence spectra measured at room temperature of sample S-3 annealed in different conditions as well as the CL spectrum of sample S-3, also acquired at room temperature, annealed at 900 °C for 60 s. The PL spectra are similar to the CL spectra, being the violet band at 400 nm the dominant luminescence emission. Therefore, the same excitation paths seem to be involved in both PL and CL cases. The recombination mechanism responsible for the emission should also be the same as in CL. The clear improvement of the luminescence emission as the annealing temperature and time are increased due to the improvement of the crystalline quality of the nanocrystals, with the corresponding reduction of the influence of the non-radiative recombination mechanisms.

4. Conclusions

Intense luminescence emission peaking at 400 nm is obtained from multilayer structures with SiGe nanocrystals embedded in a SiO_2 matrix obtained by LPCVD of amorphous SiGe nanoparticles and a subsequent thermal annealing for their crystallization. The highest intensity of this emission is obtained in samples with small SiGe nanocrystals (3–4.5 nm) separated by thick oxide barriers (≈35 nm), annealed at 900 °C for 60 s. These conditions represent a good compromise between the appropriate crystallization of the small nanoparticles and their reduced compositional degradation by Ge diffusion, due to the thick SiO_2 interlayers that act as a barrier to such diffusion. The samples show cathodoluminescence and photoluminescence emission at 400 nm both at 80 K and at room temperature. The intensity of the luminescence is increased by 25–30% after a subsequent annealing of the samples at 450 °C in forming gas.

References

M. Zacharias, L.X. Yi, J. Heitmann, R. Scholz, M. Reiche, U. Gösele, Solid State Phenom. 94 (2003) 131.
T.Z. Lu, M. Alexe, R. Scholz, V. Telelaev, M. Zacharias, Appl. Phys. Lett. 87 (2005) 202110.
S.N.M. Mestanza, E. Rodríguez, N.C. Frateschi, Nanotechnology 17 (2006) 4548.
T. Stoica, E. Sutter, Nanotechnology 17 (2006) 4912.
M.I. Ortiz, J. Sangrador, A. Rodríguez, T. Rodríguez, A. Kling, N. Franco, N.P. Barradas, C. Ballesteros, Phys. Stat. Sol. (a) 203 (2006) 1284.
M.I. Ortiz, A. Rodríguez, J. Sangrador, T. Rodríguez, M. Avella, J. Jiménez, C. Ballesteros, Nanotechnology 16 (2005) S197.
M. Avella, A.C. Prieto, J. Jiménez, A. Rodríguez, J. Sangrador, T. Rodríguez, Solid State Commun. 136 (2005) 224.
G.V.M. Williams, A. Bittar, H.J. Trodahl, J. Appl. Phys. 67 (1990) 1874.
M. Zacharias, P. Streintenberger, Phys. Rev. B 62 (2000) 8391.
I.H. Campbell, P.M. Fauchet, Solid State Commun. 58 (1986) 739.
Á.C. Prieto, Á. Torres, J. Jiménez, A. Rodríguez, J. Sangrador, T. Rodríguez, J. Mater. Sci. : Mater. Electron. 19 (2008) 155.